FERMILAB
MAR 1 10
LIBRARY
Fermilab Library
0 1160 0072932 1
TRI-PP-95-4

TRI-PP-95-4
Feb 1995

A Simulation Platform for the Design of Position Encoding Multicrystal Detectors

G. Tsang, C. Moisan, and J. G. Rogers
TRIUMF, 4004 Wesbrook Mall, Vancouver B.C., Canada V6T 2A3

submitted to IEEE Transactions on Nuclear Science

Abstract

We introduce a platform developed to simulate the measured performance of position encoding multicrystal detectors for imaging applications. The platform is designed to treat simultaneously the interactions of γ-rays in an inorganic scintillator, the geometry of the multicrystal array, as well as the propagation and detection of individual scintillation photons. Energy and position spectra predicted by the simulation are compared to measured ones for the block detectors of the ECAT EXACT HR PLUS positron emission tomograph.

I. Introduction

Recently, fast inorganic scintillators with high light yield, such as YAP [1], LSO [2] or LuAP [3] have become available. Although the improvement in energy and time resolution is clear from measurements taken on small individual crystals, the overall performance of multicrystal arrays made of newly available scintillators is difficult to assess because of their relatively high cost per unit volume compared to the wide spread BGO. With prices well above one dollar per gram, the search for the multicrystal geometry and signal readout configuration achieving optimal energy and position resolution simply can not be afforded on an empirical trial and error basis. Yet there is little hope to see a significant drop in their purchase price without demand driven by the development of position encoding detectors for commercial use. A dedicated simulation platform then becomes an attractive tool to bring down the time and material invested in the development phase of a new block and to guarantee the satisfactory performance of the early prototype.

We present a platform designed to simulate the performance of position encoding multicrystal detectors. The initial development of the platform has focussed on the simulation of the standard commercial block manufactured by Siemens-CTI for the ECAT EXACT HR PLUS positron emission tomograph. In the following sections we first present the conceptual design of the platform. The methods to measure the block energy and position responses are also briefly presented. Results of the simulation are then compared to the measurements. Finally, we discuss the actual limitations of the platform and its future prospects.

II. The Simulation Platform

Figure 1 shows the conceptual design of the simulation platform. The platform is designed to treat simultaneously the interactions of γ-rays in an inorganic scintillator, the geometry of the multicrystal array, as well as the propagation and detection of individual scintillation photons.

The geometry of the block is first used as input to the "γ-ray transport module". A uniform beam of γ-rays with specified energy is generated from a distant point source. Each incident photon is then tracked in the volume of the block for photoelectric and Compton interactions. Cross-sections for these two processes are derived from GEANT [4] for the inorganic scintillator considered in the block design. Their relative ratio is used to randomly choose which of the two processes occurs, and the flight path of the interacting γ is randomly generated according to an exponential distribution. The total cross-section at the energy of the interacting γ determines the interaction length of the exponential. Values of the cross-sections are tabulated from 15 to 511 keV in bins of 5 keV. Tracking is stopped either by a photoelectric interaction, escape of the photon from the block volume, or by a Compton interaction leaving less than 15 keV to the recoil photon. For Compton interactions, the direction of the scattered γ follows the Klein-Nishina angular distribution and the energy of the recoil electron is assumed to be converted to light at the interaction vertex. Scattering of γ's into the detector block from the cannister or surrounding supports is not modelled.

For each interaction, an "event scintillation vector" is written to a "γ-ray interaction list file". The first three words are the coordinates of the interaction point within the block volume (X_i, Y_i, Z_i). The fourth word gives the calibrated light yield at that vertex, L_i, while the last word is a sequential index incremented for each interaction until all the energy of the incoming γ is deposited in the block volume.

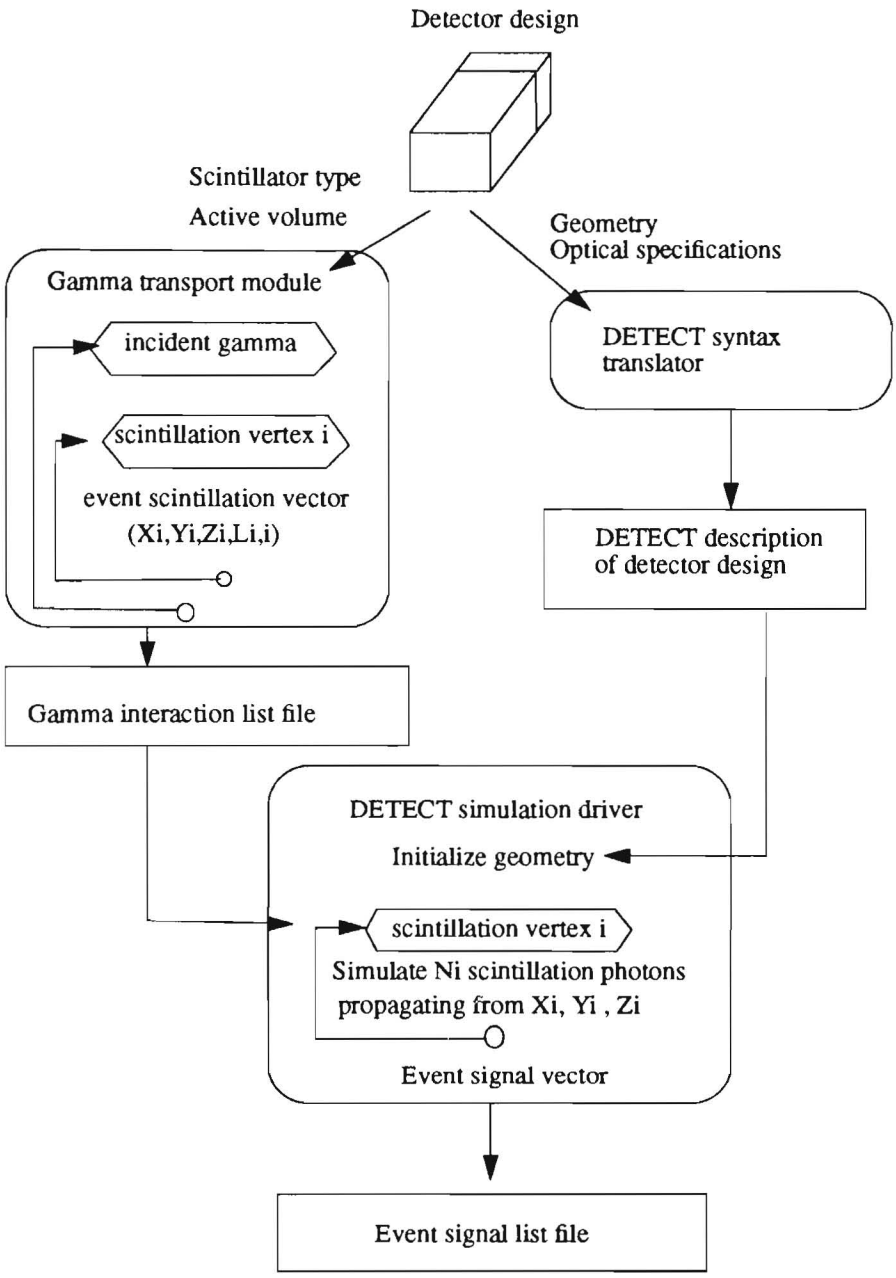

Figure 1: Data flow diagram of the block simulation platform

"The DETECT syntax translator" describes the geometry and optical properties of the block in adherence to the language syntax imposed by the light transport simulator DETECT [5]. DETECT is capable of realistically modelling the behaviour of scintillation detectors. Individual scintillation photons are isotropically generated in a specified voxel of the active volume of the detector and tracked throughout their passage within the elements or "components" of the block as well as their interactions with the surfaces. Optical tracking is pursued until a photon is either absorbed at the surface or in the active material; reaches one or more detection elements; or escapes from the detector volume. The program allows the geometry of the detector to be described with a very general syntax. Components of the detector can be specified by connecting surfaces that are either planar, cylindrical, conical or spherical. The optical properties of individual surfaces may be specified to simulate polished, ground, painted or metalized finishes; each possessing its own characteristic reflection coefficient and angular distribution.

Once the geometry and optics of the detector is translated according to DETECT's syntax, it is included in the "DETECT simulation driver" to initialize the block design specifications. Scintillation events from the γ-ray interaction list file are then simulated sequentially. The coordinates (X_i, Y_i, Z_i) of the interaction point are used to specify an infinitesimal voxel from which L_i scintillation photons are isotropically generated and tracked by DETECT. The signals collected in each of the detection elements of the detector are written in an "event signal vector" along with the coordinates and index of the scintillation. Event signal vectors belonging to the same incoming γ-ray are finally merged to compute a record encoding the total energy left in the detector, and the coordinates of the interaction. Monte Carlo information from the event scintillation vectors may also be duplicated. The resulting "signal list file" is then stored on disk for subsequent data analysis.

III. Validation with the ECAT EXACT HR PLUS Block

The standard commercial BGO block detector manufactured by Siemens-CTI for the ECAT EXACT HR PLUS scanner was chosen as a first validation test for the simulation. A detailed account of the performances of this block has recently been presented by Cherry *et al.* in [6]. The block has dimensions of $36\times38\times30$ mm^3. The light yield from interacting γ-rays is read by an assembly of four circular photomultiplier tubes (PMT) of 1" diameter coupled to the back face of the BGO block. Saw cuts perpendicular to the PMT's entrance windows segment the block into an 8×8 crystal matrix for position encoding. The edge and corner crystals of the block are cut slightly smaller than the other detectors to maintain centre-to-centre crystal spacing between blocks in a ring tomograph.

A. *Block performance measurements*

To allow a validation of the simulation platform the energy and position response functions of a prototype block were measured on a crystal-by-crystal basis. For these measurements, 511 keV γ-rays from a 0.3 mCi point source of ^{68}Ge were used in a benchtop setup described in detail elsewhere [7]. Source and detector were held at a distance of about 40 cm to obtain a uniform flood of single γ-rays at the block front face. The sum of the four PMT signals, $(A+B+C+D)$, was thresholded and used to drive the trigger logic. For each trigger, the signal from each PMT was acquired from a 10-bit ADC with an integration time of 1000 nsec. The four ADC conversions were available for subsequent processing.

The energy of an incident γ-ray, E_γ, and its coordinates in the transverse plane of the block, (X_γ, Y_γ), are computed from the PMT signals according to:

$$E_\gamma = A+B+C+D\,, \tag{1}$$

$$X_\gamma = \frac{(B+D)-(A+C)}{A+B+C+D}\,, \tag{2}$$

$$Y_\gamma = \frac{(A+B)-(C+D)}{A+B+C+D}\,. \tag{3}$$

The gains of the PMT's were balanced by requiring that the inclusive count rates be equal within statistics in each quadrant of the block. With typically 10000 counts per quadrant, this represents a 1% tolerance on the relative gain balance. Once the gains were balanced, a high statistics data run was acquired with the flood source to perform the block position calibration. The relationship between measured and true interaction positions is non-linear in position encoding BGO block detectors [7, 8]. A lookup table is therefore necessary to relate a given (X_γ, Y_γ) pair to crystal row and column addresses. Such a lookup table was obtained with the high statistics run according to the procedure introduced in [7]. Crystal-by-crystal energy spectra were consequently derived from the same data run.

B. *Block specifications for DETECT*

Table 1 lists the input parameters used to describe the block geometry and optical properties with DETECT.

The scintillation light yield of the crystal was taken from the measured value of 8200 $\pm$350 $\pm$400 photons/MeV reported in [9]. The BGO sample used in the production of the HR PLUS block is characterized by an index of refraction of 2.14 [10]. Derenzo and Riles [11] have measured a total attenuation length, λ_t, of 200 mm at the peak emission wavelength in clear BGO crystals. Nowadays, improvements in crystal growing methods provide much clearer BGO samples, and total attenuation length values are quoted to be as high as 2000 mm [10]. To allow for bulk absorption as well as scattering in the simulation, this value was split in two equal components, λ_a, and λ_s,

parameter	Input Value
BGO light yield	8200 photons/MeV
BGO refraction index	2.14
BGO scattering length	4000 mm
BGO absorption length	4000 mm
surface finish	polished
surface reflectivity	85%
block dim (mm)	36(T)×38(A)×30(H)
block segmentation	8×8
adjacent crystal spacing (mm)	0.46(T)×0.46(A)
PMT photocathode radius	7.5 mm
PMT window refraction index	1.52
photocathode quantum eff.	0.11

Table 1: List of input parameters used to describe the optical properties of BGO as well as the block detector geometry with DETECT.

of 4000 mm, in agreement with the ansatz:

$$\frac{1}{\lambda_t} = \frac{1}{\lambda_a} + \frac{1}{\lambda_s}. \tag{4}$$

In DETECT, three different options: "ground", "painted" and "polished" could potentially model the surface finish and coating of the block. To see which of these is realistic, a 30 mm long crystal centred on a detection unit was simulated. The finish of the five faces of the crystal not in contact with the detection unit was considered to be either ground, painted or polished and coated by an opaque reflector with a reflection coefficient of 85% [10]. A point source was moved in steps of 1 mm across the length of the crystal, starting at 1 mm from the top up to the position of the detection unit. The simulated photon yield in the detection unit is presented as a function of the source position in Figure 2 for all three surface finishes. All simulated data points were normalized to the total photon yield of 100% at the position of the detection unit. The results from the simulation are compared to the dependence, measured by Cherry et al. [6], for a crystal at the centre of the HR PLUS block, of the photopeak energy channel upon the longitudinal position of interacting gamma-rays. The polished finish exhibits a dependence matching well the data measured by Cherry. Using ground and painted finishes causes a dependence of the light collection upon the longitudinal position of the source that is incompatible with measurements. On the basis of this comparison, the surface finish of the HR PLUS crystals was specified to DETECT as being polished with a reflection coefficient of 85%.

To allow for saw cut recesses varying for different crystal rows or columns, the geometry specification of the block had to be partitioned into a number of components much larger than the number of crystals. The cut depths were assumed to be axially and transaxially symmetrical. In that case, a crystal is a stack of four components, one for

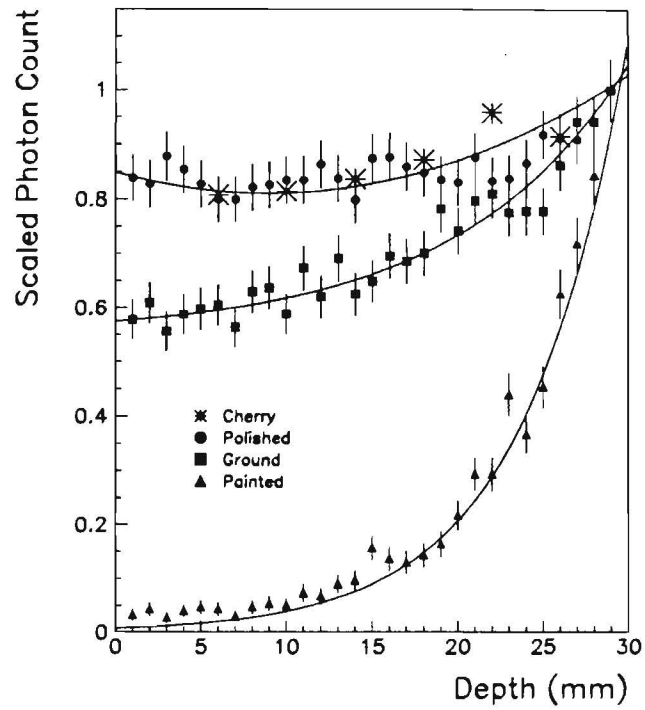

Figure 2: The normalized photon yield as a function of longitudinal source position, or "depth", in a 30 mm long crystal for three different surface finish models in DETECT compared to measurements for a crystal at the centre of the HR PLUS block.

each bounding sides' cut depths. The volumes beneath the cuts had to be separated into their own components as well. Adding to this the components that define the four PMT's, a total surpassing 500 components is required for the block geometry declaration to DETECT. Interactions located within the volume of the saw cuts, taken to be 0.46 mm wide, were ignored by the DETECT simulation driver. DETECT rejects any scintillation locations lying outside the specified geometry and automatically reports zeros for the PMT counts. Null signal events are subsequently filtered out by lower energy thresholding.

To acquire the capacity of determining saw cut recesses providing good crystal position identification is one of the principal aims of the simulation platform. Values of the cut depths for the simulated 2D flood position reconstruction map were therefore inferred through optimization. The optimization process begins with setting all the cut depths to zero. Each cut is then systematically lowered starting from the outside towards the centre. The optimal depth of the cut for the simulation is reached when the peak of the position distribution for events in the crystal defined by the cut is well resolved from its inner and outer neighbours. Due to the four-fold symmetry of the block, the optimization only considered crystals along the diagonal of one quadrant. The search process can be further quickened by simulating a small set of 511 keV-equivalent photon point sources in

a given crystal. Point sources were spread along the longitudinal axis of the crystal within the mean attenuation length of 511 keV photons in BGO and the average of the reconstructed positions gave a good approximation of the peak location. Even though the peak locations in the reconstruction map match well the measured locations, the peak-to-valley ratios may be unacceptably inconsistent. As a result, once a preliminary set of cut depths is found, a full simulation of the 16 crystals in a quadrant is still needed. Fine adjustments to the cut depths are finally made to improve the ratios. This last step again involves using a 511 keV-equivalent point source and exploits the empirical fact that as the cut recesses are lowered, the peaks shift towards the edge of the block and become better resolved.

The geometry of the PMT's was modelled after the Hamamatsu R5364. The model consisted of a cylinder with a flat top and spherical detection surface at the bottom representing the photocathode. The inner cylindrical wall was given a 100% reflective mirror finish and the top surface was assumed to be polished with an index of refraction of 1.52. The cylinder length of 1.5 mm and radius of 7.5 mm were taken from the Hamamatsu catalog diagram of the R5364. The radius of curvature of the photocathode was chosen such that it came within 0.1 mm of the top surface. To simulate the entrance window of the PMT's and the optical glue coupling the PMT's to the BGO block, four glass plates were used with dimensions of $19 \times 18 \times 0.5$ mm^3. The top and bottom faces of the plates were specified as polished. This coupling interface allows for a crosstalk of a few percent of the total signal between the PMT reading directly an edge or corner crystal and the other PMT's. The thickness of the plate was chosen to reproduce this relative signal sharing by matching the observed width of the edge crystals position response function.

The average quantum efficiency of the PMT's was derived from the integration of the normalized emission spectrum of BGO with the spectral response of bialkali photocathodes. An allowable range of $11\% \leq Q.E. \leq 14\%$ was determined from which a value of 11% was selected for the model.

The full simulation of the block detector is extremely CPU intensive. The worst case involves the optical tracking of 4190 scintillation photons from the photoelectric interaction of a 511 keV γ-ray. In that case, approximately $\frac{1}{2}$ or $1\frac{1}{3}$ minutes of CPU time is needed on a DEC Station 3000/400 or a VAX Station 4000/100 respectively. This corresponds to 2 minutes in real-time under normal system load in both cases. The four-fold symmetry of the block was exploited by folding the events into only one quadrant. A typical run consisting of a thousand gamma interactions in each crystal of one quadrant then takes around three days to complete when the tasks are distributed among three DEC Station 3000/400's and three VAX Station 4000/100's.

C. Results

Figure 3 presents the simulated energy spectra for 16 crystals in one quadrant of the block.

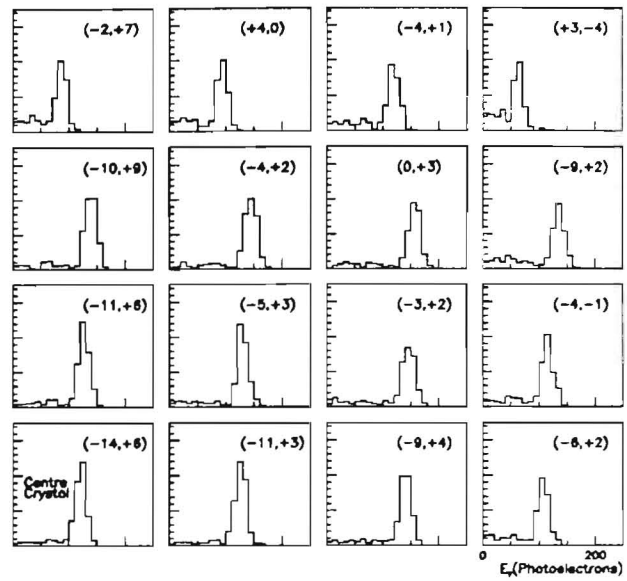

Figure 3: Simulated energy spectra for the 16 crystals in one quadrant of the block. The lower left spectrum is that of the crystal at the centre of the block. The numbers in parenthesis are absolute differences between the measured and simulated photopeak position and FWHM normalized to the crystal in the third row and third column from the centre.

The lower left spectrum belongs to the crystal at the centre of the block. For each crystal, the absolute difference between the measured and simulated photopeak position and FWHM are given in parenthesis. Values are percentages derived from:

$$\left(\frac{P^{ij}_{exp}}{P^{33}_{exp}} - \frac{P^{ij}_{sim}}{P^{33}_{sim}} \, , \, \frac{FWHM^{ij}_{exp}}{P^{ij}_{exp}} - \frac{FWHM^{ij}_{sim}}{P^{ij}_{sim}} \right) , \qquad (5)$$

where P^{ij} denotes the photopeak channel of the crystal in the ith row and j^{th} column. For the simulated data, events were assigned to the crystal in which the energy weighted centroid of interaction was located. Photopeak channels were normalized to the value obtained for the crystal in the third row and third column from the centre. Simulated and measured data were respectively normalized to the same crystal. For both simulated and measured data, this crystal presents the maximum photopeak channel.

The simulation reproduces well the crystal-by-crystal variations of the energy spectra. For most crystals, the simulated energy resolution on the photopeak is within $\pm 4\%$ of its expected value. This indicates that the combination of the BGO light yield, PMT quantum efficiency and crystal surface finish reproduces effectively the measured total photostatistics for incident 511 keV γ-rays in

the block. The simulation also predicts the measured relative position of the peaks to within the range: −14% to +4%.

Crystals near the corner have their photopeak channel (FWHM) systematically underestimated (overestimated) by the simulation while those closer to the centre tend to be overestimated (underestimated). The discrepancy increases as the crystal's location gets closer to the centre of the block. This is believed to be due to different cut depths along X and Y to achieve uniform light sharing in the HR PLUS block, which is not simulated. The simulation assumes XY-symmetrical cut depths for simplicity of the block's geometry declaration.

Finally, the familiar Compton tail of the energy spectra is well modelled. At low energy, the contribution of events escaping the block through the back plane or from the side walls is apparent in each crystal. For crystals in the inner rows and columns, the simulated ratio of the Compton plateau to the photopeak is $\sim 1/10$, in good agreement with the measured data. As expected, the Compton tail is more prominent for crystals in the edge row and column of the quadrant as more events can scatter out of the block active volume. The measured Compton yield of those crystals remains however significantly underestimated. This is not surprising, as inward scattering from the detector cannister and surrounding supports is not modelled.

Figure 4 presents the simulated 2D flood position calibration spectrum for 16 crystals in one quadrant of the block. The scale of the contour plot was chosen to enhance the view of the crystals at the centre. As a result, the good separation of the crystals in the block's edge row is masked by the expanded scale.

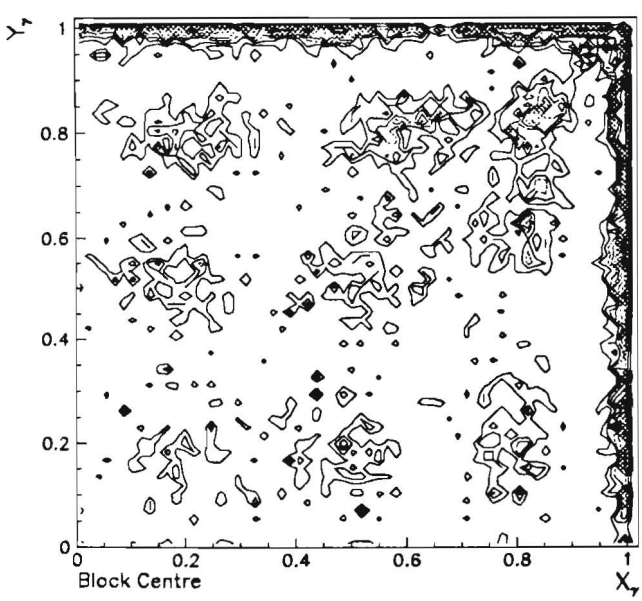

Figure 4: Simulated 2D flood position calibration spectrum for the 16 crystals in one quadrant of the block.

The simulated flood spectrum shows 16 resolved crystal peaks in the (X_γ, Y_γ) space. This indicates that our choice of cut depths effectively models the relative optical coupling of individual crystals to each of the four PMT's. Detailed features of the measured flood position calibration spectrum of the HR PLUS block [6] are also well reproduced. The simulated data show the typical pin cushion deformation stretching the inner crystal peaks towards the outmost corner of the block. Furthermore, in the HR PLUS block, optical cross-talk between the PMT's through a common entrance window is more suppressed than in previous block designs [7]. As a result, peaks belonging to the edge rows and columns do not move inward towards the centre of the edge rows. Figure 4 shows that this new feature is well reproduced by the simulation.

Figure 5 allows a more quantitative appreciation of the simulation accuracy in reproducing the measured flood position map. The figure presents a comparison between the simulated (a) and measured (b) position peaks for a row of crystals at the centre of the block. Only events with more than 350 keV were selected. The integral of counts was normalized to unity in both cases. The simulated spectrum is symmetrical with respect to the centre and was also smoothed to avoid artifacts from low statistics.

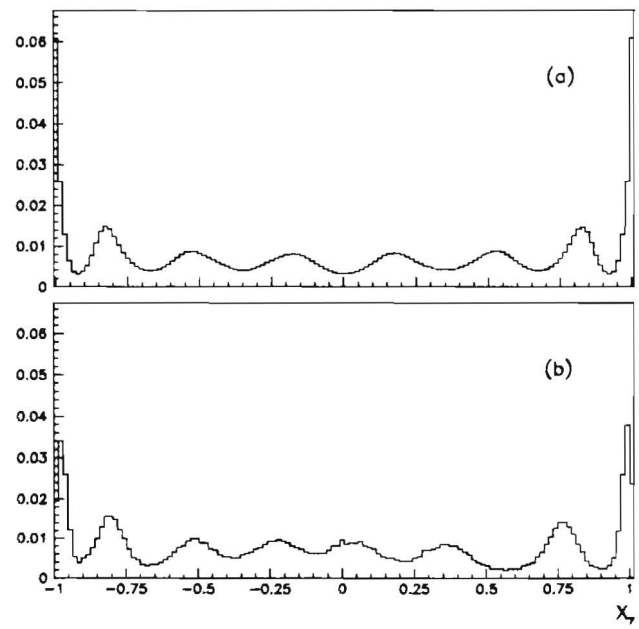

Figure 5: Comparison between simulated (a) and measured (b) position map for a row of crystals at the centre of the block.

Even though the experimental spectrum displays a slight gain imbalance which pulls the peaks towards the left of the block, one can see that the simulation models well the relative features of each peak. For crystals in the inner columns, the simulation successfully predicts the relative yield and width of the position peaks. In both simulated and measured data, the crystals in the two central columns

have a relative peak intensity of 0.009, while those of the third column have one of 0.015. At the centre of the block, the peak to valley ratio is slightly better in the simulated spectrum. The simulation is also optimistic in its prediction of the position response of the edge crystals. It overestimates the peak yield by a factor 2 and underestimates its width.

A possible explanation of this is the following. For events in the edge crystals, signal sharing is a few percents more important in the real block than what is predicted by the simulation. This is attributed to an inaccurate modelling of the optical coupling between the BGO block and the PMT's. For instance, values for the coupling glue's thickness, index of refraction, as well as absorption and scattering mean free paths were not considered. At the cost of simplicity, the coupling plate used in the simulation to effectively model the PMT entrance window could have better been sectioned into separate components for the glue and the PMT window, each with their own characteristics.

IV. Discussion and Conclusions

In this work we introduced a simulation platform dedicated to the simulation of multicrystal position encoding scintillation detectors. The principal feature of the platform is to interface γ-ray interactions with the propagation and detection of optical photons. The former is determined by the bulk properties of the inorganic scintillator and allows to realistically model the deposition of energy in the active volume of the block through photoelectric and Compton interactions. The latter is dominated by the geometry and optical properties of the saw-cut multicrystal array as well as by the PMT coupling scheme. Combining the two clearly provides an optimization tool more realistic than geometrical and optical optimization alone.

The platform was put to a first test by comparing the predicted energy and position spectra to those measured for an ECAT EXACT HR PLUS block. With a simple and realistic treatment of the block geometry and optics, the relative features of the various crystal energy spectra were well reproduced. The measured crystal-by-crystal photopeak channels and energy resolutions were respectively predicted to a good accuracy. Similarly, the simulated 2D flood position calibration spectrum reproduced detailed features of the measured one. The relative intensities of the peaks and valleys, as well as the widths of the peaks in the position map were shown to agree well with measurements except for a minor disagreement on the edge crystals.

The prediction power of the platform is now to be further confirmed by the successful design of a yet unexisting block prototype. In this respect, the potential of the simulation is opened to many avenues. As mentioned in the introduction, the design of multicrystal position encoding detectors based on new high light yield inorganic scintillators is surely an important application. Block designs capable of simultaneously good transverse and Depth-of-Interaction resolutions, either through surface treatment [12] or novel readout schemes [13], also deserve attention. Finally, the capacity of the platform to tackle γ-ray and light transport together makes it a good tool to study event miscoding in existing or future block designs which might lead eventually to energy and position encoding algorithms of better resolution.

V. Acknowledgements

The authors want to thank T. A. DeVol of Clemson University for providing them with the source code and user manual for DETECT. This study would not have been possible without S. R. Cherry of UCLA who lent us the HR EXACT PLUS blocks he received from CTI. The collaboration of R. Nutt, M. Andreaco and C. W. Williams of Siemens-CTI, where the detectors were fabricated was also much appreciated.

Glenn Tsang and Christian Moisan acknowledge the Natural Sciences and Engineering Research Council of Canada for its support through postgraduate and postdoctoral fellowships respectively.

References

[1] S. I. Ziegler, J. G. Rogers, V. Selivanov and I. Sinitzin, "Characteristics of New $YAlO_3$:Ce Compared with BGO and GSO", IEEE Trans. Nucl. Sci., **NS-40** 194 (1993).

[2] C. L. Melcher and J. S. Schweitzer, "Cerium-doped Lutetium Oxyorthosilicate: A fast, efficient new scintillator", IEEE Trans. Nucl. Sci., **NS-39** 502 (1992).

[3] W. W. Moses, S. E. Derenzo, A. Fyodorov, M. Korzhik, A. Gektin and B. Minkov, "$LuAlO_3$:Ce- A High Density, High Speed Scintillator for Gamma Detection", to appear in the proceedings of the 1994 IEEE Medical Imaging Conference of Norfolk, Norfolk, Virginia, Nov 3-5 1994.

[4] R. Brun, F. Bruyant, M. Maire, A. C. McPherson and P. Zanarini, "GEANT3", CERN Data Handling Division, DD/EE/84-1, September 1987.

[5] G. F. Knoll, T. F. Knoll and T. M. Henderson, "Light Collection Scintillation Detector Composites for Neutron Detection", IEEE Trans. Nucl. Sci., **NS-35** 872 (1988).

[6] S. R. Cherry, M. P. Tornai, C. S. Levin, S. Siegel and E. J. Hoffman, "A Comparison of PET Detector Modules Employing Rectangular and Round Photomultiplier Tubes", to appear in the proceedings of the 1994 IEEE Medical Imaging Conference of Norfolk, Norfolk, Virginia, Nov 3-5 1994.

[7] J. G. Rogers, A. J. Taylor, M. F. Rahimi, R. Nutt, M. Andreaco and C. W. Williams, "An improved multicrystal 2-D BGO detector for PET", IEEE Trans. Nucl. Sci., **NS-39** 1063 (1992).

[8] J.G.Rogers, R.Nutt, M.Andreaco and C.W.Williams, "Testing 144- and 256-crystal BGO block detectors", IEEE Trans. Nucl. Sci., **NS-41** 1423 (1994).

[9] I. Holl, E. Lorenz and G. Mageras, "A Measurement of the Light Yield of Common Inorganic Scintillators", IEEE Trans. Nucl. Sci., **NS-35** 105 (1988).

[10] Private communication, CTI PET Systems, Inc., 810 Innovation Drive, Knoxville, Tennessee, USA.

[11] S. E. Derenzo and J. K. Riles, "Monte Carlo Calculation of the Optical Coupling Between Bismuth Germanate crystals and Photomultiplier Tubes", IEEE Trans. Nucl. Sci., **NS-29** 191 (1982).

[12] J. G. Rogers, "A method for correcting the Depth-of-Interaction blurring in PET cameras", to appear in IEEE Trans. Med. Imag. (in press).

[13] W. W. Moses and S. E. Derenzo, "Design studies for a PET detector module using a PIN photodiode to measure depth of interaction.", IEEE Trans. Nucl. Sci., **NS-41** 1441 (1994).

NAME | DATE | M.S.

RETURN TO FERMILAB LIBRARY